Journal of Solid State Chemistry 202 (2013) 154–160

Contents lists available at SciVerse ScienceDirect

Journal of Solid State Chemistry

journal homepage: www.elsevier.com/locate/jssc

New quinternary selenides: Syntheses, characterizations, and electronic structure calculations

Ming-Yan Chung, Chi-Shen Lee *

Department of Applied Chemistry, National Chiao Tung University, 1001 University Road, Hsinchu 30010, Taiwan

ARTICLE INFO

Article history:
Received 17 December 2012
Received in revised form
5 March 2013
Accepted 12 March 2013
Available online 26 March 2013

Keywords:
Selenide
Quinternary
Site preference
Alkaline earth metal
Rare earth metal

ABSTRACT

Five quinternary selenides, $Sr_{2.63}Y_{0.37}Ge_{0.63}Sb_{2.37}Se_8$ (**I**), $Sr_{2.63}La_{0.37}Ge_{0.63}Sb_{2.37}Se_8$ (**II**), $Sr_{2.71}La_{0.29}Sn_{0.77}Bi_{2.23}Se_8$ (**III**), $Ba_{2.67}La_{0.33}Sn_{0.67}Sb_{2.33}Se_8$ (**IV**), and $Ba_{2.67}La_{0.33}Sn_{0.67}Bi_{2.33}Se_8$ (**V**), were synthesized by solid-state reaction in fused silica tubes. These compounds are isostructural and crystallize in the $Sr_3GeSb_2Se_8$ structural-type, which belongs to the orthorhombic space group *Pnma* (no. 62). Three structural units, $^1_\infty[MSe_3]$, $^1_\infty[M_4Se_{10}]$ (M=*Tt*, *Pn*) and M' (M'=groups **II** and **III** element), comprise the entire one-dimensional structure, separated by M'. Measurements of electronic resistivity and diffused reflectance suggest that **IV** and **V** have semiconducting properties. Electronic structure calculations confirm the site preferences of Sr/La element discovered by crystal structure refinement.

1. Introduction

Multinary chalcogenides play an increasingly important role in solid-state physics, chemistry, and materials science. Among these materials, chalcogenides containing alkali, alkaline earth, and rare earth elements have received attention for their diverse structures and applications in thermoelectric (TE) devices [1–5] and nonlinear optics [6–8]. These materials' chemical and physical properties can be manipulated by modifying the cation and chalcogen anion substitutions. Chalcogenides incorporating group **1**, **2**, or rare earth elements usually provide rich coordination environments for the main group elements, and have low structural dimensionalities. These features generally reduce thermal conductivity, and may enhance thermoelectric properties [3]. Combining the chalcogenides with other p-block elements, such as Ge, Sn, or Pb from group 14, or the elements Sb or Bi from group 15, results in the formation of various anionic frameworks that can function as building blocks in the formation of new structures with different coordination numbers [9–15].

Many quinternary chalcogenides have been studied during the past decade. The first published example was $K_{0.5}Ba_{0.5}DyCu_{1.5}Te_3$ [16]. The complex $A_{5-x}K_{1+x}Sn[Zn_4Sn_4S_{17}]$ (A=K^+, Rb^+, Cs^+; x=0, 4, 5)[17] exhibits a chalcogen-based open framework with interesting ion-exchange properties. Quinternary minerals with complex components have been studied, including angelaite [18], billingsleyite [19], watlinsonite [20], and cosalite [21]. Unlike other quinternary systems, $KCaEr_2CuS_5$ [22] is the first reported quinternary sulfide that does not exhibit substitutional disorder.

Our group has studied a number of multinary metal selenides representative of several different systems, including *Tr*–*Tt*–*Pn*–Se [23], *TM*–*Tr*–*Tt*–Se [24], and *Ae*–*Tt*–*Pn*–Se systems [25] (*Ae*=alkaline earth elements; *TM*=transition metal; *Tr*=In; *Tt*=Sn, Pb; *Pn*=Sb, Bi). Our studies of these systems revealed a charge-balanced system $Ae_3SnPn_2Se_8$ (*Ae*=Sr, Ba, *Pn*=Sb, Bi) [26] featuring tetrahedrally coordinated Bi atoms. We investigated an *A*–*M*–*Q* (*A*=alkali, alkaline earth, or rare earth metal; *M*=group 3–5 p-block metal; *Q*=S, Se, Te) series analogous to this system, and report the synthesis of five quinternary selenides. We present their syntheses, structures, physical properties, and calculations of their electronic structures. Sr and La metal sites exhibit substitutional disorder in *M*1–3 sites, with site preferences determined by single-crystal X-ray diffraction. These measurements are further supported by electronic structure calculations.

2. Experimental

2.1. Synthesis

All compound preparations were performed in a glove box under a dry nitrogen atmosphere. Chemicals were used as obtained (from Alfa Aesar)—Ba chunks, 99.00%; Sr chunks, 99.00%; Ge powder, 99.50%; Sn powder, 99.80%; Sb powder, 99.90%; Bi powder, 99.50%; Se powder, 99.95%; Y chunks, 99.00%; La chunks, 99.00%. All reactions were

* Corresponding author. Fax: +886 3 5723764.
E-mail addresses: chishen@mail.nctu.edu.tw, chishenlee@gmail.com (C.-S. Lee).

0022-4596/$ - see front matter © 2013 Elsevier Inc. All rights reserved.
http://dx.doi.org/10.1016/j.jssc.2013.03.025

conducted using reagents in their elemental forms, in fused silica tubes placed in a temperature-controlled furnace.

In attempts to synthesize analogous compounds to $Sr_8YGe_2Bi_7Se_{24}$ [26], we combined pure elements in the appropriate stoichiometric ratios by weight (total mass approximately 0.5 g) under a dry nitrogen atmosphere following the general formula $Ae_8MTt_2Pn_7Se_{24}$ (Ae=Sr, Ba; M=Y, La; Tt=Ge, Sn; Pn=Sb, Bi). Reaction mixtures were heated to 1023 K over one day, maintained at that temperature for one day, slowly cooled to 673 K over a day, and finally cooled to room temperature (approximately 300 K) by terminating the power. The products were polycrystalline ingots that exhibited a metallic luster. Those were powdered before characterization by powder X-ray diffraction. The powder X-ray diffraction patterns for reaction mixtures $Sr_8YGe_2Sb_7Se_{24}$, $Sr_8LaGe_2Sb_7Se_{24}$, $Sr_8LaSn_2Bi_7Se_{24}$, $Ba_8LaSn_2Sb_7Se_{24}$, and $Ba_8LaSn_2Bi_7Se_{24}$ showed peaks corresponding to the $Sr_3GeSb_2Se_8$ [25] structure. After structural determination from single-crystal X-ray diffraction data, we obtained refined formulas for these new compounds, which are $Sr_{2.63}Y_{0.37}Ge_{0.63}Sb_{2.37}Se_8$ (**I**), $Sr_{2.63}La_{0.37}Ge_{0.63}Sb_{2.37}Se_8$ (**II**), $Sr_{2.71}La_{0.29}Sn_{0.77}Bi_{2.23}Se_8$ (**III**), $Ba_{2.67}La_{0.33}Sn_{0.67}Sb_{2.33}Se_8$ (**IV**), and $Ba_{2.67}La_{0.33}Sn_{0.67}Bi_{2.33}Se_8$ (**V**). Subsequent attempts to synthesize pure phases of compounds **I**–**V** were conducted using the mentioned reaction conditions. Powder X-ray diffraction measurements showed that samples **IV** and **V** were in good agreement with their calculated patterns, indicating pure phases for these compounds (Figs S4 and S5). However, the compositions of **I**, **II**, and **III** respectively produce a minor phase of Sb_2Se_3, Sb_2Se_3, and Bi_2Se_3 (Figs. S1–3).

3. Characterization

Powder X-ray diffraction was performed by a Bruker D8 Advance diffractometer (operated at 40 kV and 40 mA, with Cu $K\alpha$ radiation, λ=1.5418 Å). The data were collected over a 2θ range of 5–60° in 0.016° steps, with an exposure time of 0.1 s per step. Diffuse reflectance measurements were conducted using a UV–visible spectrophotometer (Jasco V-670). Ground powder samples were placed into a thin glass slide holder, and a $BaSO_4$ plate served as a reference. An integrating sphere was used to measure the diffuse reflectance spectra over the range 200–2000 nm. The band gap was determined by extrapolating the linear regions of each $(\alpha/s)^2$ versus energy plot to $(\alpha/s)^2$ to zero. Differential thermal analysis (DTA) data were obtained on a thermal analyzer (NETZSCH STA 409PC). A small quartz tube with an inner diameter (i.d.)=3 mm was filled with roughly 50 mg of the sample, sealed under vacuum, and placed into the analyzer. DTA data were collected by heating to 1073 K and cooling to 673 K at a rate of 10 K/min under a constant flow of nitrogen gas. Electrical resistivity measurements were performed using the standard four-probe method on a cold pressed bar ($1\times1\times5$ mm^3). Each sample bar was annealed at 673 K for one week before measurement.

3.1. Single-crystal X-ray diffraction

Single crystals were obtained from the crushed reaction products and mounted on the ends of glass fibers for single-crystal X-ray diffraction studies. Intensity data were collected on a diffractometer (Bruker APEX CCD equipped with graphite-monochromated Mo–$K\alpha$ radiation, λ=0.71073 Å) at 293(2) K. Crystals were positioned 5.0 cm from the detector. Data were collected by scans of 0.3° in ω in groups of 600 frames at φ settings of 0° and 60°. The 2θ values varied between 2.74° and 56.56°. Diffraction signals obtained from 80 frames of reciprocal-space images were used to determine unit-cell parameters. The APEX 2 program package, including SAINT and SHELXTL, was used for structure determination and refinement [27]. Absorption corrections were based on fitting a function to the empirical transmission surface, as sampled by multiple equivalent measurements of numerous reflections.

3.2. Calculation of electronic structure

The calculation of electronic structure was performed by self-consistent tight-binding first principle LMTO (linear muffin tin orbitals) calculations using the atomic spheres approximation (ASA) [28–32]. We applied density functional theory using local density approximation (LDA) in the LMTO approximation. To study the influence of M (M=Y, La) substitution and preference to the refined crystal structure, three models were constructed to represent different conditions of occupation for La and Sr atoms. Those models were based on the refined crystal structure of $Sr_{2.67}La_{0.33}Sn_{0.67}Bi_{2.33}Se_8$ and its b-axis was extended to a triple cell with the $Pna2_1$ space group. The general formula is $Sr_8LaSn_2Bi_7Se_{24}$. All independent crystallographic sites were triplicated and categorized as a, b, and c sites. For example, in a triple cell, the $M1$ site in the origin cell is split into three sites, named $M1a$,

Table 1
Crystal data and structure refinement for compounds **I**–**V**.

	I	**II**	**III**	**IV**	**V**
Refined composition	$Sr_{2.63}Y_{0.37}Ge_{0.63}Sb_{2.37}Se_8$	$Sr_{2.63}La_{0.37}Ge_{0.63}Sb_{2.37}Se_8$	$Sr_{2.71}La_{0.29}Sn_{0.77}Bi_{2.23}Se_8$	$Sr_{2.67}La_{0.33}Sn_{0.67}Sb_{2.23}Se_8$	$Ba_{2.66}La_{0.33}Sn_{0.67}Bi_{2.33}Se_8$
Temperature	293(2) K	293(2) K	293(2) K	293(2) K	293(2) K
Wavelength	0.71073 Å	0.71073 Å	0.71073 Å	0.71073 Å	0.71073 Å
Crystal system	Orthorhombic	Orthorhombic	Orthorhombic	Orthorhombic	Orthorhombic
Space group, Z	*Pnma* (62), 4	*Pnma* (62), 4	*Pnma* (62), 4	*Pnma* (62), 4	*Pnma* (62), 4
a/Å	12.594(3)	12.537(3)	13.047(4)	12.630(3)	13.062(3)
b/Å	4.3323(9)	4.348(1)	4.262(1)	4.626(1)	4.4596(9)
c/Å	28.862(6)	28.812(6)	29.220(9)	29.628(8)	29.892(6)
V/Å^3	1574.7(6)	1570.7(6)	1624.7(8)	1731.1(8)	1735(1)
θ_{min}, θ_{max}/deg	1.41/25.02	1.41/25.02	1.71/25.02	1.37/25.03	1.36/25.03
Independent reflections (R_{int})	1587 (0.0476)	1581 (0.0353)	1637 (0.0595),	1746 (0.0341),	1759 (0.0467)
observed reflections	13602	13638	13211	14988	15229
d_{calcd}/mg m^{-3}	3.883	3.946	5.177	4.050	4.609
Absorption coefficient/mm^{-1}	25.378	25.194	40.682	21.074	35.897
Goodness-of-fit on F^2	1.110	1.102	1.066	1.106	1.040
R_1, wR_2 ($I>2s(I)$)	0.0364, 0.0792	0.0376, 0.0884	0.0279, 0.0591	0.0467, 0.1140	0.0393, 0.0870
R_1, wR_2 (all data)[a]	0.0474, 0.0841	0.0422, 0.0908	0.0368, 0.0625	0.0503, 0.1164	0.0454, 0.0907
Largest diff. peak and hole/eÅ^{-3}	3.316, −3.196	3.110, −3.157	1.826, −3.057	4.234, −5.375	5.5058, −3.350

[a] $R_1=\sum||F_0|-|F_c||/\sum|F_0|$ $wR_2=\{\sum(w(F_0^2-F_c^2)^2)/\sum(w(F_0^2)^2)\}^{1/2}$

Table 2
Atomic coordination, equivalent isotropic displacement parameters and site occupancy factors (SOF) of **I**–**V**.

Site	*X*	*Y*	*z*	U_{eq}[a]	SOF
I					
M(1*A*)	0.0308(1)	0.75	0.4115(1)	0.026(1)	Sr/Y 0.80/0.11
M(2)	0.6950(1)	0.75	0.3439(1)	0.019(1)	Sr/Y 0.88/0.12
M(3)	0.3292(1)	0.75	0.3149(1)	0.019(1)	Sr/Y 0.88/0.12
M(4)	0.0702(2)	0.25	0.2819(1)	0.044(1)	Ge/Sb 0.63/0.37
Sb(5)	0.4535(1)	0.25	0.4327(1)	0.026(1)	Sb 1.00
Sb(6)	0.7649(1)	0.25	0.4718(1)	0.032(1)	Sb 1.00
Se(1)	0.8522(1)	0.25	0.3884(1)	0.019(1)	Se 1.00
Se(2)	0.5022(1)	0.25	0.3442(1)	0.018(1)	Se 1.00
Se(3)	0.1622(1)	0.25	0.3569(1)	0.022(1)	Se 1.00
Se(4)	0.3169(1)	0.75	0.4245(1)	0.030(1)	Se 1.00
Se(5)	0.2644(1)	0.25	0.2624(1)	0.022(1)	Se 1.00
Se(6)	0.6189(1)	0.75	0.4500(1)	0.045(1)	Se 1.00
Se(7)	0.8985(2)	0.75	0.5058(1)	0.054(1)	Se 1.00
Se(8)	0.4710(2)	0.75	0.2209(1)	0.094(1)	Se 1.00
M(1*B*)	0.0091(1)	0.75	0.4412(7)	0.013(3)	Sr/Y 0.07/0.01
II					
M(1)	0.0323(1)	0.75	0.4127(1)	0.029(1)	Sr/La 0.87/0.13
M(2)	0.6969(1)	0.75	0.3439(1)	0.020(1)	Sr/La 0.87/0.13
M(3)	0.3297(1)	0.75	0.3150(1)	0.019(1)	Sr/La 0.87/0.13
M(4)	0.0685(1)	0.25	0.2818(1)	0.044(1)	Ge/Sb 0.61/0.39
Sb(5)	0.4537(1)	0.25	0.4327(1)	0.026(1)	Sb 1.00
Sb(6)	0.7654(1)	0.25	0.4725(1)	0.030(1)	Sb 1.00
Se(1)	0.8543(1)	0.25	0.3886(1)	0.019(1)	Se 1.00
Se(2)	0.5032(1)	0.25	0.3441(1)	0.018(1)	Se 1.00
Se(3)	0.1620(1)	0.25	0.3569(1)	0.023(1)	Se 1.00
Se(4)	0.3163(1)	0.75	0.4243(1)	0.029(1)	Se 1.00
Se(5)	0.7357(1)	0.25	0.2622(1)	0.024(1)	Se 1.00
Se(6)	0.6190(1)	0.75	0.5501(1)	0.047(1)	Se 1.00
Se(7)	0.8987(2)	0.75	0.5058(1)	0.053(1)	Se 1.00
Se(8)	0.4695(2)	0.75	0.2797(1)	0.093(1)	Se 1.00
III					
M(1)*A*	0.0254(4)	0.75	0.4123(2)	0.018(1)	Sr/La 0.70/0.17
M(2)	0.6904(1)	0.75	0.3470(1)	0.019(1)	Sr/La 0.98/0.02
M(3)	0.3247(1)	0.75	0.3170(1)	0.023(1)	Sr/La 0.92/0.08
M(4)	0.0639(1)	0.25	0.2803(1)	0.031((1)	Sn/Bi 0.77/0.23
Bi(5)	0.4492(1)	0.25	0.4351(1)	0.017(1)	Bi 1.00
Bi(6)	0.7671(1)	0.25	0.4758(1)	0.020(1)	Bi 1.00
Se(1)	0.8500(1)	0.25	0.3882(1)	0.017(1)	Se 1.00
Se(2)	0.4973(1)	0.25	0.3429(1)	0.015(1)	Se 1.00
Se(3)	0.1562(1)	0.25	0.3582(1)	0.019(1)	Se 1.00
Se(4)	0.3077(1)	0.75	0.4245(1)	0.017(1)	Se 1.00
Se(5)	0.2313(1)	0.25	0.2354(1)	0.022(1)	Se 1.00
Se(6)	0.6145(1)	0.75	0.4527(1)	0.018(1)	Se 1.00
Se(7)	0.8985(1)	0.75	0.5067(1)	0.018(1)	Se 1.00
Se(8)	0.4467(1)	0.75	0.2209(1)	0.047(1)	Se 1.00
M(1*B*)	0.9992(9)	0.75	0.4329(4)	0.020(3)	Sr/La 0.11/0.03
IV					
M(1)	0.0457(1)	0.75	0.4137(1)	0.037(1)	Ba/La 0.89/0.11
M(2)	0.7096(1)	0.75	0.3433(1)	0.021(1)	Ba/La 0.89/0.11
M(3)	0.3382(1)	0.75	0.3144(1)	0.022(1)	Ba/La 0.89/0.11
M(4)	0.0753(1)	0.25	0.2849(1)	0.046(1)	Sn/Sb 0.67/0.33
Sb(5)	0.4619(1)	0.25	0.4312(1)	0.037(1)	Sb 1.00
Sb(6)	0.7680(1)	0.25	0.4713(1)	0.042(1)	Sb 1.00
Se(1)	0.8608(1)	0.25	0.3921(1)	0.023(1)	Se 1.00
Se(2)	0.5141(1)	0.25	0.3454(1)	0.022(1)	Se 1.00
Se(3)	0.1751(2)	0.25	0.3590(1)	0.042(1)	Se 1.00
Se(4)	0.3309(2)	0.75	0.4258(1)	0.059(1)	Se 1.00
Se(5)	0.2559(2)	0.25	0.2618(1)	0.026(1)	Se 1.00
Se(6)	0.6233(2)	0.6631(5)	0.5482(1)	0.027(1)	Se 1.00
Se(7)	0.8981(3)	0.75	0.5050(1)	0.104(2)	Se 1.00
Se(8)	0.4715(2)	0.75	0.2854(1)	0.066(1)	Se 1.00
V					
M(1)	0.0296(1)	0.75	0.4123(1)	0.029(1)	Ba/La 0.89/0.11
M(2)	0.6938(1)	0.75	0.3458(1)	0.018(1)	Ba/La 0.89/0.11
M(3)	0.3262(1)	0.75	0.3143(1)	0.019(1)	Ba/La 0.89/0.11
M(4)	0.0636(1)	0.25	0.2813(1)	0.038(1)	Sn/Bi 0.67/0.33
Bi(5)	0.4491(1)	0.25	0.4340(1)	0.026(1)	Bi 1.00
Bi(6)	0.7635(1)	0.25	0.4747(1)	0.033(1)	Bi 1.00
Se(1)	0.8494(1)	0.25	0.3910(1)	0.020(1)	Se 1.00
Se(2)	0.5004(1)	0.25	0.3450(1)	0.017(1)	Se 1.00
Se(3)	0.1621(2)	0.25	0.3575(1)	0.025(1)	Se 1.00
Se(4)	0.3122(2)	0.75	0.4252(1)	0.024(1)	Se 1.00

Table 2 (*continued*)

Site	*X*	*Y*	*z*	U_{eq}[a]	SOF
Se(5)	0.2308(2)	0.25	0.2366(1)	0.025(1)	Se 1.00
Se(6)	0.6116(2)	0.75	0.4542(1)	0.028(1)	Se 1.00
Se(7)	0.8954(2)	0.75	0.5065(1)	0.044(1)	Se 1.00
Se(8)	0.4525(2)	0.75	0.2156(1)	0.066(1)	Se 1.00

[a] U_{eq} is defined as one third of the trace of the orthogonalized U_{ij} tensor.

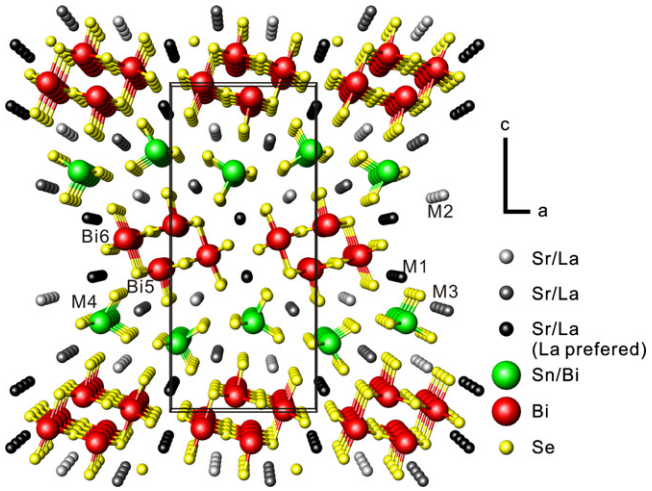

Fig. 1. Perspective view of the structure of $Sr_{2.71}La_{0.29}Sn_{0.77}Bi_{2.23}Se_8$ (**III**) along the *b*-axis.

*M*1*b*, and *M*1*c*. All nine possible Sr/La models were calculated. Considering the relative energies, models 1–3 were isolated to represent La occupying the *M*1–3 sites, respectively (Table S2). The integrations of *k* space were on grids containing more than 300 independent *k* points within the first Brillouin zone.

4. Results and discussion

4.1. Crystallographic study

All crystal samples possessed orthorhombic unit-cell parameters similar to $Sr_3GeSb_2Se_8$ [25]. The systematic absence condition suggested two possible space groups, *Pnma* (no. 62) and $Pna2_1$ (no. 33), from which we chose *Pnma* because the refinement gave the best structural model. Direct method gave an initial model with 14 independent crystallographic sites: three *M*1–3 are *Ae* or *M* (*Ae*=Sr, Ba; *M*=Y, La), one *M*4 for *Tt* (*Tt*=Ge, Sn), two *M*5–6 for *Pn* (*Pn*=Sb, Bi), and eight sites for Se. For the crystal data of **I** and **III**, the differential Fourier maps indicate significant electron densities close to the *M*1 site, indicative of split sites. These were named *M*1B and were constrained with the *M*1*A* site. For crystal data of **IV**, we refined *M*4 and *M*5–6 sites as Sn/Sb (0.67/0.33) and a fully occupied Sb, whereas *M*1–3 sites were constrained with a Ba/La ratio of 89/11. For crystal data of **I**, **III**, and **V**, the *M*4 site was refined as mixed-occupation Ge/Sb or Sn/Bi, whereas site occupancy factor (SOF) refinement of *M*5–6 sites gave 100% Sb or Bi. The *M*4 in **V** was freely refined as 62.1/37.9 (Sn/Bi), close to 0.67/0.33 of Sn/Bi. SOF refinement of **III**s *M*1–3 and *M*4 sites were refined freely as Sr/La (*M*1–3) and Sn/Bi (*M*4). For compounds **I** and **V**, the compositions of the *M*1–3 sites were fixed according to the Ge/Sb or Sn/Bi ratio to maintain charge balance. The final refined formulas were $Sr_{2.63}Y_{0.37}Ge_{0.63(1)}Sb_{2.37(1)}Se_8$ (**I**), $Sr_{2.63}La_{0.37}Ge_{0.63(2)}Sb_{2.37(2)}Se_8$ (**II**), $Sr_{2.71(2)}La_{0.29(2)}Sn_{0.77(1)}Bi_{2.23(1)}Se_8$ (**III**), $Ba_{2.67}La_{0.33}Sn_{0.67}Sb_{2.33}Se_8$ (**IV**), and $Ba_{2.662}La_{0.33}Sn_{0.66}Bi_{2.33}Se_8$ (**V**). These formulas are close to the charge-balanced formula $Ae_{2.67}M_{0.33}Tt_{0.67}Pn_{2.33}Se_8$ (*Ae*=Sr, Ba; *M*=Y, La; *Tt*=Ge, Sn; *Pn*=Sb, Bi). The final refinement yielded *R*-values of approximately 0.04. The results of the crystallographic studies are listed in Tables 1 and 2, and S1. The calculations of bond valance sums [33] of **I**–**V** were summarized in Table S2.

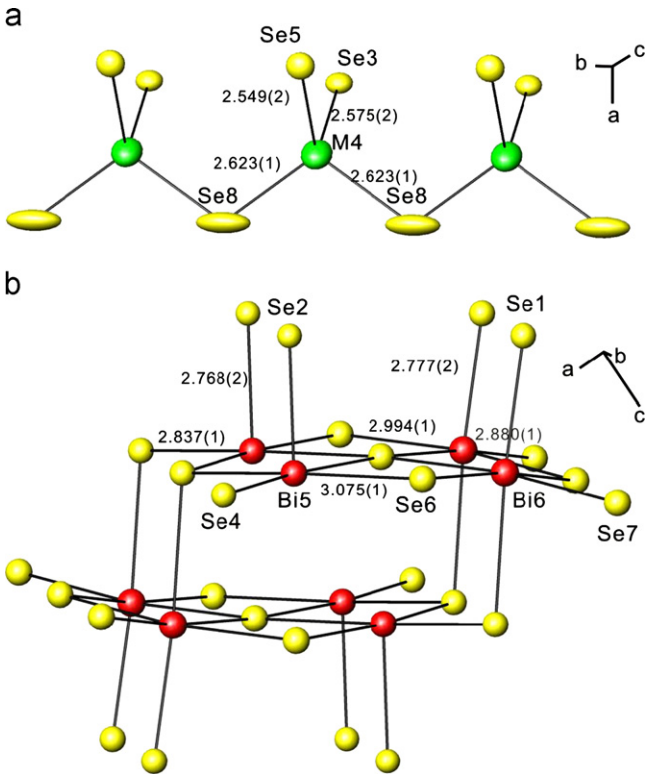

Fig. 2. Ellipsoid-plots of (a) $^1_\infty[MSe_3]$ and (b) $^1_\infty[Bi_4Se_{10}]$ units in **III**.

In an attempt to observe the possible super cell structure in this system [26], low-temperature (110 K) crystal data were collected. The reconstructed zone images and RLATT analysis did not show evidence for superstructure diffraction. The low-temperature refinements produced similar results to those for room temperature studies. Thus, these compounds do not form a superstructure.

4.2. Structural description

$Ae_{2.67}M_{0.33}Tt_{0.67}Pn_{2.33}Se_8$ (*Ae*=Sr, Ba; *M*=Y, La; *Tt*=Ge, Sn; *Pn*=Sb, Bi) are all isostructal with $Sr_3GeSb_2Se_8$ [25]. We present the structural details of **III** as a representative structure sample. There are 14 independent crystallographic sites: three are Sr/La (*M*1–3), one is Sn/Bi (*M*4), two are Bi (Bi5–6), and eight are Se (Se1–8). Fig. 1 shows a perspective view of the structure along the *a*-axis. There are two types of one-dimensional structural units: $^1_\infty[MSe_3]$ (*M*4) and $^1_\infty[Bi_4Se_{10}]$ (Bi5–6) (Fig. 2). For the $^1_\infty[MSe_3]$ unit, tetrahedral MSe_4 interlinks through two corners. For the $^1_\infty[Bi_4Se_{10}]$

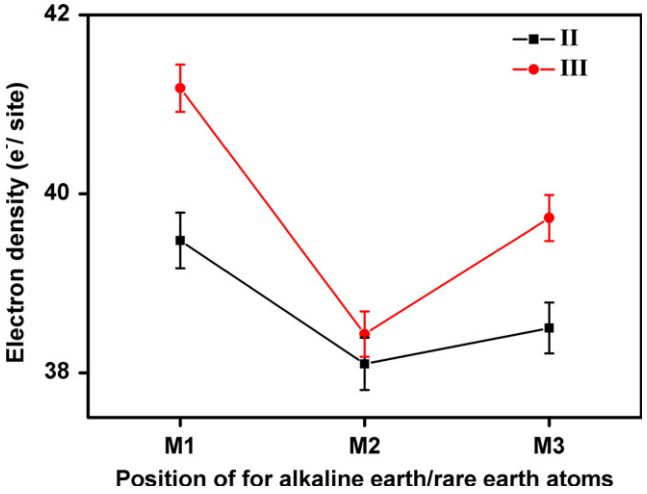

Fig. 3. Refined electron density for *M*1–3 sites for $Sr_{2.63}La_{0.37}Ge_{0.63}Sb_{2.37}Se_8$ (**II**) and $Sr_{2.71}La_{0.29}Sn_{0.77}Bi_{2.23}Se_8$ (**III**).

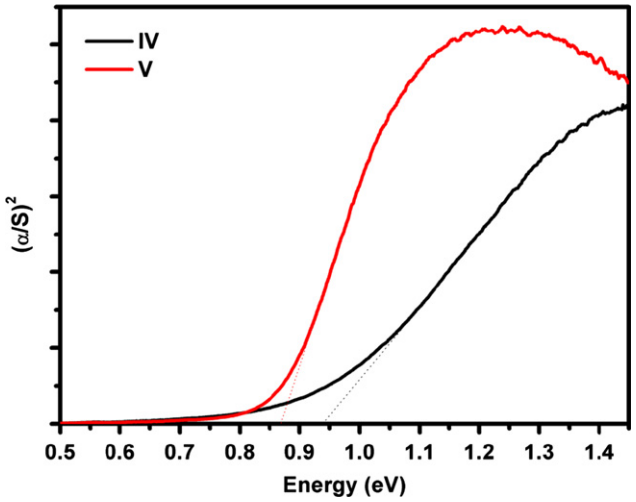

Fig. 4. Diffuse reflectance spectra for **IV** (black) and **V** (red). (For interpretation of the references to color in this figure legend, the reader is referred to the web version of this article.)

unit, octahedral $BiSe_6$ connects by shared edges. These two one-dimensional units are separated by Sr/La (*M*1–3).

The alkaline earth *Ae* (*Ae*=Sr, Ba) and rare earth *M* (*M*=Y or La) atoms occupy *M*1–3 sites. The refined electron densities of *M*1–3 sites are different. The electron densities of *M*1–3 sites are greater than 38 (Sr) and less than 57 (La), suggesting mixed occupation by La and Sr cations. Fig. 3 shows the *M*1–3 electronic densities for compounds **II** and **III**, determined by SXRD refinement. The electron density at the *M*1 site is significantly greater than those at the *M*2 and *M*3 sites, indicating a greater concentration of La atoms in *M*1 compared to those at *M*2 and *M*3 sites. Thus, the La atom preferentially occupies the *M*1 site. Substitution of La by Sr also affects the electron densities of *M*6 sites for main group elements. In this study, the electron densities of *M*6 sites in compound **III** are 80.4 e^-/site, which is greater than that of $Sr_3SnBi_2Se_8$ [26] at 78.6 e^-/site. These results suggest that electron density increases at *M*6 sites when La is substituted in the *M*1–3 sites. Similar features were seen for compound **II**.

*M*1–3 sites are located in bi-capped trigonal prism environments and occupied by Sr/La at ratios of 80/20 (*M*1), 98/2 (*M*2), and 92/8 (*M*3). The *M*–Se contacts range from 3.18 to 3.71 Å (*M*1–Se), 3.21 to 3.88 Å (*M*2–Se) and 3.15 to 3.42 Å (*M*3–Se). Compared to some strontium and lanthanide selenides, these contacts are 3.15 to 3.58 Å for $SrBi_2Se_4$ [34] and 3.03 to 3.49 Å for $La_4FeSb_2Se_{12}$ [12], respectively. The *M*4 site has a mixed occupation with a Sn/Bi ratio of 77/23. The coordination environment at the M4 site is a distorted tetrahedron with *M*–Se contacts ranging from 2.54 to 2.62 Å, slightly greater than the range of Sn–Se distances seen for Ba_2SnSe_5 (2.50–2.59 Å) [35], because of the greater atomic radius of the Bi atom. The Bi5–6 sites are located in distorted octahedral sites with 100% Bi. The Bi5 site has three shorter (2.77–2.84 Å), two middle (3.07 Å), and one remote (3.38 Å) contact, whereas Bi6–Se contacts range from 2.78 to 3.07 Å, comparable to Bi–Se contacts in Bi_2Se_3 and related phases [34].

4.3. Physical Properties

Diffused reflectance studies were conducted to determine the optical band gaps of compounds **IV** and **V**. Fig. 4 shows plots of reflectance versus photon energy. The measured optical band gaps were approximately 0.94 eV for **IV** and 0.87 eV for **V**.

The activation energy was estimated through temperature-dependent electronic resistivity using the four-probe method (Fig. 5). Resistivity progressively decreased with decreasing temperature for **IV** and **V**, indicative of semiconducting behavior. The

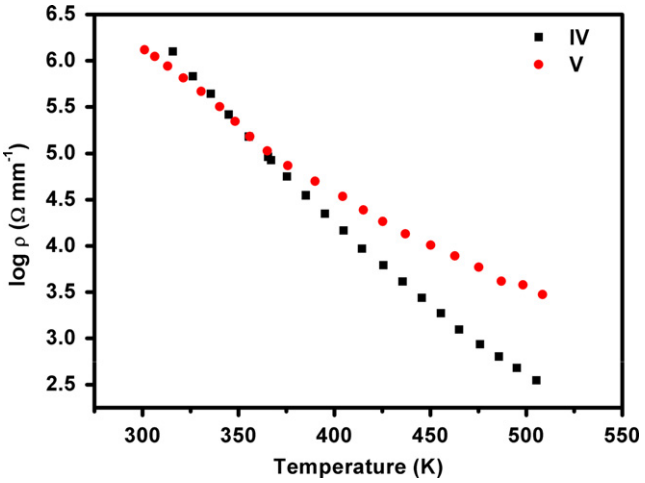

Fig. 5. Electrical resistivity of $Ba_{2.67}La_{0.33}Sn_{0.67}Sb_{2.33}Se_8$ (**IV,** black) and $Ba_{2.67}La_{0.33}Sn_{0.67}Bi_{2.33}Se_8$ (**V,** red). (For interpretation of the references to color in this figure legend, the reader is referred to the web version of this article.)

calculated activation energies for **IV** and **V** were 0.81 and 0.52 eV, respectively, consistent with band gap trends seen in diffuse reflectance measurements.

The DTA curves indicate that the melting temperatures of **IV** and **V** are 970 and 1130 K, respectively (Fig. S3). The melting temperatures of the La substituted compounds increased by 60 and 20 K, compared to $Ba_3SnBi_2Se_8$ and $Ba_3SnSb_2Se_8$ [26], respectively, because of the effect of La substitution in **IV** and **V**.

4.4. Electronic structure

According to the refined SXRD data for **II** and **III**, La preferentially occupies the *M*1 site, over the *M*2 and *M*3 sites. To understand the site preference for *M*1–3 sites in $Ae_{2.67}M_{0.33}Tt_{0.67}Pn_{2.33}Se_8$, we constructed a lower symmetry model with space group $Pna2_1$ and tripling the unit cell *b* to simulate a partially occupied *M*4 site (0.66 Sn/0.33 Bi). The coordination and constituent elements were based on crystal data from compound **III**. We constructed three hypothetical models representing La occupations at *M*1, *M*2, and *M*3 sites, with a general formula $Sr_8LaSn_2Bi_7Se_{24}$. Details of those models are listed in Table S3.

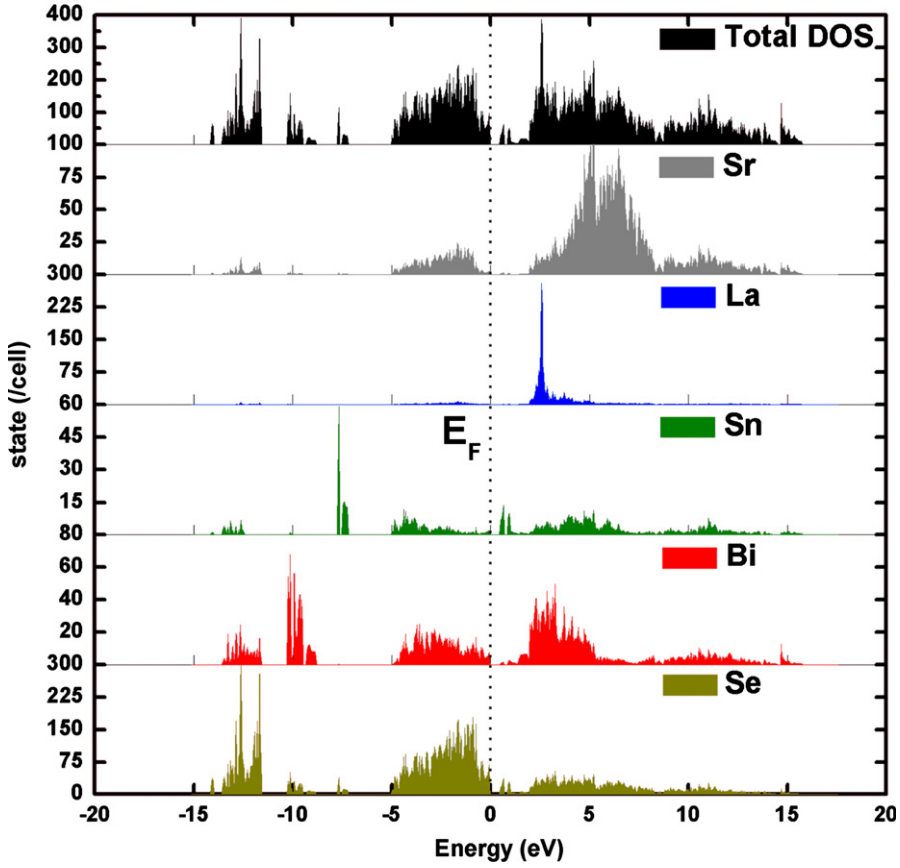

Fig. 6. Total and partial densities of states for $Sr_{2.67}La_{0.33}Sn_{0.67}Bi_{2.33}Se_8$ (Model 1).

All models produced similar results regarding their band structures and DOS (densities-of-states) curves (Fig. 6 and S4). Model **1** exhibits the lowest total energy of all models; this is discussed below. The total and partial DOS of $Sr_8LaSn_2Bi_7Se_{24}$ (**1**) are shown in Fig. 5. The calculated band gap is approximately 0.48 eV, indicative of semiconducting properties. The Sr, La, Sn, and Bi np states contribute to the valance band between zero and −5 eV, which is a consequence of covalent mixing with Se 4*p* states. The ns states of all atoms are located below −5 eV. The major contributors to the conduction band are Sr 4*d* and La 4*f* states, which are distributed over ranges of 3–15 eV and 3–5 eV, respectively. Sn, Bi, and Se make minor contributions to the conduction band.

The effects of La substitution at *M*1–3 sites on the relative total energies of these models are plotted in Fig. 7. The results show that the relative total energy of **1** with La atom occupancy at the M1 site, roughly 2 eV/cell, is significantly less than that of either **2** (La occupancy at *M*2) or **3** (La occupancy at *M*3). This indicates that the model with La substitution of the M1 site is more stable than La substitution at *M*2 and *M*3 sites. This might arise from differences between local environments at *M*1–3 sites. Interatomic distances of *M*1–Se are generally shorter than those of *M*2–Se and *M*3–Se for 6-coordinated trigonal-prismatic environments. The ionic radius of La^{3+} is less than that of Sr^{2+}, and thus, La^{3+} ions are able to access more sterically hindered coordination sites. Our site preference study of electronic structure calculation supports the results of SOF based on single-crystal X-ray diffraction data (Fig. 3).

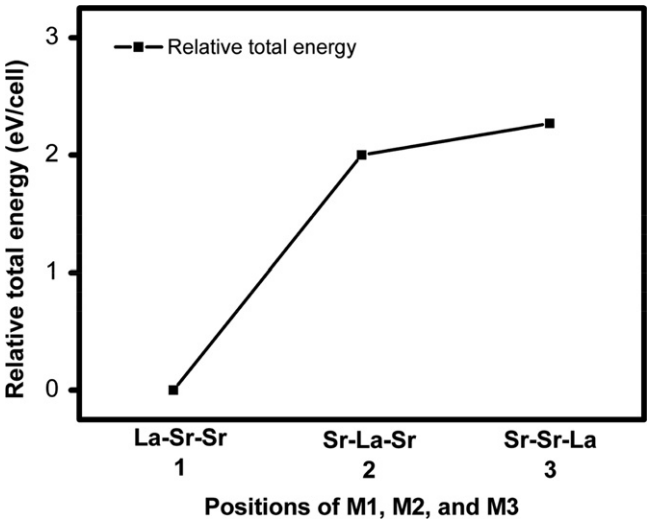

Fig. 7. Relative total energy for models with La occupancy in position *M*1 (**1**), *M*2 (**2**), and *M*3 (**3**) sites. The sequence of La and Sr in parenthesis denotes positions of *M*1, *M*2, and *M*3.

5. Conclusion

Five quinternary selenides, $Sr_{2.63}Y_{0.37}Ge_{0.63}Sb_{2.37}Se_8$ (**I**), $Sr_{2.63}La_{0.37}Ge_{0.63}Sb_{2.37}Se_8$ (**II**), $Sr_{2.71}La_{0.29}Sn_{0.77}Bi_{2.23}Se_8$ (**III**), $Ba_{2.67}La_{0.33}Sn_{0.67}Sb_{2.33}Se_8$ (**IV**), and $Ba_{2.67}La_{0.33}Sn_{0.67}Bi_{2.33}Se_8$ (**V**), were synthesized and characterized. These complexes are isostructural with $Sr_3GeSb_2Se_8$, and are constructed from $^1_\infty[MSe_3]$ (M= *Tt*/*Pn*), $^1_\infty[Bi_4Se_{10}]$ units, and *Ae*/*M*′ atoms (*Ae*=Sr, Ba; *M*′=Y, La). The Sr positions can be partially substituted by rare earth La, which alters the composition of metal sites for *Tt* (Ge, Sn) and *Pn* (Sb, Bi) to form a charge-balanced compound. Diffused reflectance and temperature-dependent resistivity measurements of **IV** and **V** suggested semiconductor behaviors for these compounds. The site preference of Sr/La

atoms was confirmed by single X-ray diffraction and electronic structure calculations.

Acknowledgment

We thank Professor Eric W.-G. Diau for measurements of UV diffuse reflectance. National Science Council (NSC 101-2113-M-009-017-MY3) supported this research.

Appendix A. Supporting information

Supplementary data associated with this article can be found in the online version at http://dx.doi.org/10.1016/j.jssc.2013.03.025.

References

[1] D. Chung, Science 287 (2000) 1024–1027.
[2] B.C. Sales, Science 295 (2002) 1248–1249.
[3] G.J. Snyder, E.S. Toberer, Nat. Mater. 7 (2008) 105–114.
[4] S.N. Girard, J. He, X. Zhou, D. Shoemaker, C.M. Jaworski, C. Uher, V.P. Dravid, J.P. Heremans, M.G. Kanatzidis, J. Am. Chem. Soc. 133 (2011) 16588–16597.
[5] J. He, A. Gueguen, J.R. Sootsman, J.-C. Zheng, L. Wu, Y. Zhu, M.G. Kanatzidis, V.P. Dravid, J. Am. Chem. Soc. 131 (2009) 17828–17835.
[6] I. Chung, J.-H. Song, J.I. Jang, A.J. Freeman, J.B. Ketterson, M.G. Kanatzidis, J. Am. Chem. Soc. 131 (2009) 2647–2656.
[7] B. Eisenmann, M. Jakowski, H. Schaefer, Rev. Chim. Miner. 20 (1983) 329 -37.
[8] X. Lin, G. Zhang, N. Ye, Cryst. Growth Des. 9 (2009) 1186–1189.
[9] A. Assoud, H. Kleinke, Chem. Mater. 17 (2005) 4509–4513.
[10] A. Assoud, N. Soheilnia, H. Kleinke, Chem. Mater. 17 (2005) 2255–2261.
[11] A. Assoud, K.M. Kleinke, H. Kleinke, Chem. Mater. 18 (2006) 1041–1046.
[12] Z. Huajun, L. Longhua, W. Liming, C. Ling, Inorg. Chem. 48 (2009) 11518–11524.
[13] A. Mrotzek, M.G. Kanatzidis, Acc. Chem. Res. 36 (2003) 111–119.
[14] L. Iordanidis, M.G. Kanatzidis, Inorg. Chem. 40 (2001) 1878–1887.
[15] A. Mrotzek, L. Iordanidis, M.G. Kanatzidis, Chem. Commun. (2001) 1648–1649.
[16] F.Q. Huang, W. Choe, S. Lee, J.S. Chu, Chem. Mater. 10 (1998) 1320–1326.
[17] M.J. Manos, R.G. Iyer, E. Quarez, J.H. Liao, M.G. Kanatzidis, Angew. Chem. Int. Ed. 44 (2005) 3552–3555.
[18] D. Topa, E. Makovicky, H. Putz, Can. Miner. 48 (2010) 145–153.
[19] L. Bindi, R.T. Downs, S. Menchetti, Can. Miner. 48 (2010) 155–162.
[20] D. Topa, E. Makovicky, J. Sejkora, H. Dittrich, Can. Miner. 48 (2010) 1109–1118.
[21] D. Topa, E. Makovicky, Can. Miner. 48 (2010) 1081–1107.
[22] H.-Y. Zeng, H. Mattausch, A. Simon, F.-K. Zheng, Z.-C. Dong, G.-C. Guo, J.-S. Huang, Inorg. Chem. 45 (2006) 7943–7946.
[23] M.-F. Wang, S.-M. Jang, J.-C. Huang, C.-S. Lee, J. Solid State Chem. 182 (2009) 1450–1456.
[24] K.-C. Wang, C.-S. Lee, Inorg. Chem. 45 (2006) 1415–1417.
[25] C.-Y. Yu, M.-F. Wang, M.-Y. Chung, S.-M. Jang, J.-C. Huang, C.-S. Lee, Solid State Sci. 10 (2008) 1145–1149.
[26] M.-Y. Chung, C.-S. Lee, Inorg. Chem. 51 (2012) 13328–13333.
[27] Bruker, 2006. Bruker AXS Inc. Madison, WI.
[28] O.K. Andersen, Phys. Rev. B 12 (1975) 3060.
[29] P.E. Blöhl, O. Jepsen, O.K. Andersen, Phys. Rev. B: Condens. Matter 49 (1994) 16223–16233.
[30] O. Jepsen, O.K. Andersen, Z. Phys. 97 (1995) 25.
[31] H.L. Skriver, The LMTO Method, Springer, Berlin, 1984.
[32] U. van Barth, L. Hedin, J. Phys. C 4 (1971) 2064.
[33] I.D. Brown, D. Altermatt, Acta Cryst. B 41 (1985) 244–247.
[34] Y.C. Wang, R. Hofmann, F.J. DiSalvo, J. Solid State Chem. 156 (1999) 230–236.
[35] M. Zelinska, A. Assoud, C. Graf, H. Kleinke, Inorg. Chem. 49 (2010) 1090–1093.